Analysis of Shielded Lossy Multilayered-Substrate Microstrip Discontinuities

Essam S. Tony, *Member, IEEE,* and Sujeet K. Chaudhuri, *Senior Member, IEEE*

***Abstract*—The spatial Green's function for a rectangular cavity partially filled with multiple layers of lossy dielectrics has been derived. The Green's function is used to compute the fields around a discontinuity in a transmission line. To analyze a discontinuity, the unknown surface current maintained on the microstrip discontinuity is expanded in terms of known suitable basis functions. The electric-field components in the plane of the discontinuity region are then written in terms of this current. Imposing the boundary condition that the component of the electric-field tangential to the metallization is zero yields the electric-field integral equation (EFIE). The method of moments is applied to the EFIE to obtain a system of linear equations. The resultant semianalytical expressions were used to conduct accurate modeling of a variety of structures. The validity and accuracy of this method are established through comparison with other published results. Convergence considerations are outlined and verified.**

I. Introduction

THE problem of electromagnetic (EM) propagation in stratified isotropic and anisotropic media have been studied extensively [1]–[3]. This effort has been devoted to the task of designing monolithic microwave integrated circuits (MMICs) for the use in the high-frequency ($f > 20$ GHz) region.

Initially, theoretical work on microstrip was primarily based on quasi-TEM analysis. With this technique, equivalent circuits were derived in terms of static capacitances and low-frequency impedances. Wheeler [4], [5] was the first to evaluate the static capacitance through conformal mapping and an effective dielectric-constant approach. Other works for the static analysis of gaps in microstrips [6], gaps and steps [7] and other microstrip discontinuities [8], [10] followed. This method is valid only at low frequencies, but it is the least computationally demanding technique. Full-wave three-dimensional-discretization numerical methods are considered the most versatile, as they are applicable to geometrically more complex structures at higher frequencies. Some of these numerical methods are the method of lines [11], [12], the finite-difference time-domain (FDTD) approach [13]–[15], and the transmission-line matrix method [16]. These methods, however, are quite costly in terms of their computational requirements. Full-wave spectral- and spatial-domain techniques provide a tradeoff between speed of computation and accuracy.

In most cases, MMICs with semiconductor substrates are shielded in a metallic rectangular cavity given the brittle nature of semiconductors and in order to isolate the circuit from interaction with the surrounding environment. For this reason, shielded metal–insulator–semiconductor (MIS) microstrip structures are often found in MMICs. MIS technology is used for the design of phase shifters, attenuators, and tunable filters [17], [18], as well as modeling very high-speed very large scale integration (VLSI) circuit interconnects [19], [20].

The effect of shielding on discontinuity characteristics can be significant. Considerable effects occur when the circuit is operated at a frequency close to or above the cutoff frequency of the higher order modes of the microstrip, which are essentially the cavity modes of the shielding structure. These effects are also observed when the shielding structure is close to the circuitry [21].

The treatment proposed in [21] and [22] is intended primarily for discontinuities of thin lines, as it considers only the axial component for the current. The method proposed in [23] and [24] is an efficient generalized technique for deriving the space-domain Green's function due to an arbitrarily oriented current in a shielded two-layered isotropic substrate MIS structures. This treatment considers both the axial and transverse currents and, hence, it is suitable for the treatment of discontinuities in wider lines. In this paper, the analysis presented in [24] is extended for the case of multilayered lossy substrate. The validity of this method is established through comparison with various published data. The major advantages of this method are as follows.

1) It can accommodate arbitrarily oriented current densities.
2) It is a spatial-domain analysis that is particularly suitable for highly lossy substrates.
3) As opposed to the spectral-domain techniques (SDTs), the spatial dependence of the fields of the structure under consideration are directly observable.
4) This method expresses all the unknown field amplitude coefficients in terms of the amplitude coefficients at only one layer of the substrate. Hence, regardless of the number of substrate layers, all the unknown amplitude coefficients can be evaluated by solving a 2×2 system of equations. This provides an immense reduction in the mathematical manipulation compared to other approaches.

The following two basic assumptions are made in the forthcoming analysis.

- All conductor losses are ignored. For microstrip lines, most of the fields are concentrated under the center

Manuscript received February 8, 2000.

E. S. Tony was with the Electrical and Computer Engineering Department, University of Waterloo, Waterloo, ON, Canada N2L 3G1. He is now with the Research and Development Organization, Global High Capacity Optical Transport Division, Nortel Networks, Saint John, NB, Canada E2L 4V1 (e-mail: etony@NortelNetworks.com).

S. K. Chaudhuri is with the Electrical and Computer Engineering Department, University of Waterloo, Waterloo, ON, Canada N2L 3G1 (e-mail:sujeet@maxwell.uwaterloo.ca).

Publisher Item Identifier S 0018-9480(01)02434-6.

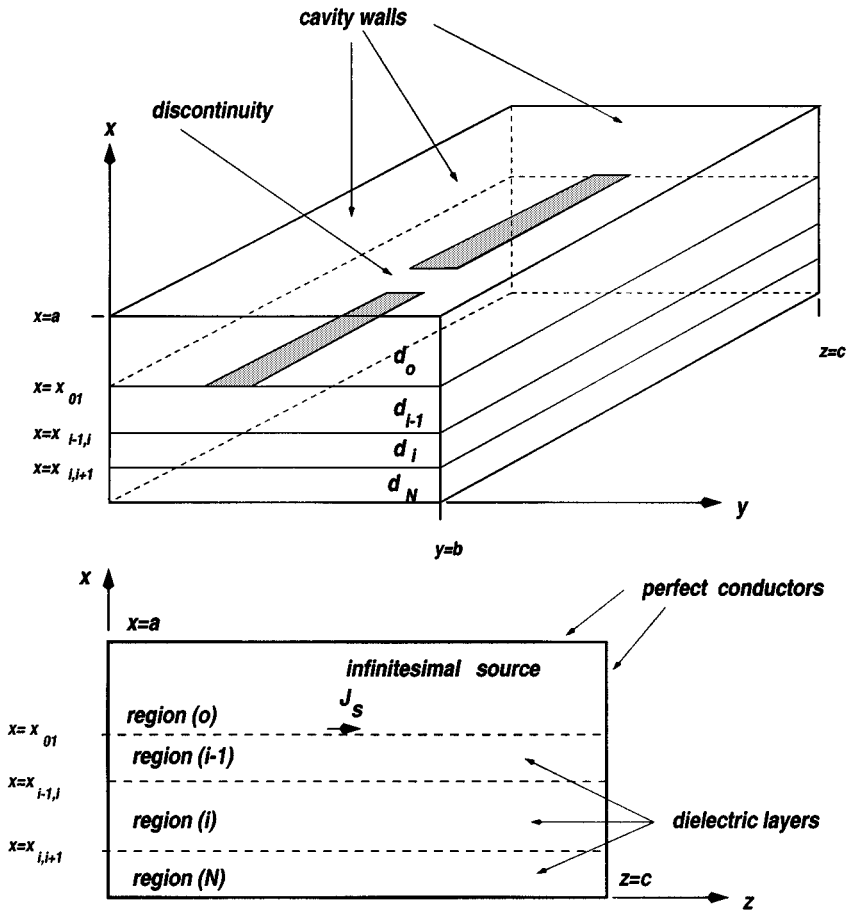

Fig. 1. Schematic of an inhomogeneously partially filled rectangular cavity.

conductor, and fringe fields attenuate rapidly away from it. Hence, losses in the shielding walls can be ignored. Microstrip metallizations are mostly made of gold, which is a very good conductor. Conductor losses are skin-effect losses that are most significant at lower frequencies ($f \leq 2$ GHz). Gold conductor losses for a line of width 500 μm is 0.01 dB/mm at 1 GHz [25]. For MIS structures, this is a negligible quantity compared to the propagation losses in the semiconductor substrates. Hence, the perfect conductor assumption is justified.

- The thickness of the microstrip metallization is assumed negligible. For an operating frequency of 20 GHz, the microwave wavelength in silicon is a few millimeters. A typical microstrip line thickness is 5 μm. Hence, the operating wavelength is at least a 1000 times bigger than the conductor thickness. Hence, the zero conductor thickness is justified.

II. Green's Function Formulation

In what follows, a procedure for deriving the electrical Green's function $G(\vec{r}, \vec{r}')$ for a multilayered structure is presented. This general procedure could be applied to a wide range of structures, e.g., an inhomogeneous dielectric-loaded rectangular cavity, as depicted in Fig. 1. The figure shows a cavity loaded with N dielectric layers and contains a point current source $\vec{J}_s(r')$ located at (x_{01}, y', z'). In response to this current source, an electric field is generated. This electric field directly yields the electric Green's function for the cavity $\vec{G}(\vec{r}, \vec{r}')$; for an arbitrary surface current $\vec{J}_s(r')$, the electric field anywhere within the cavity is given by

$$\vec{E}(\vec{r}) = -j\omega\mu_o \iint \vec{G}(\vec{r}, \vec{r}') \cdot \vec{J}_s(\vec{r}')\, ds' \tag{1}$$

where s' is the area of the surface where $\vec{J}_s(\vec{r}')\, ds'$ exists. All fields and sources are assumed to be time harmonic with a time dependence e^{jwt}. $\vec{G}(\vec{r}, \vec{r}')$ is given by

$$\begin{aligned}\vec{G}^i(\vec{r}, \vec{r}') = {} & \hat{x}\hat{y}\vec{G}^i_{xy}(\vec{r}, \vec{r}') + \hat{x}\hat{z}\vec{G}^i_{xz}(\vec{r}, \vec{r}') + \hat{y}\hat{y}\vec{G}^i_{yy}(\vec{r}, \vec{r}') \\ & + \hat{y}\hat{z}\vec{G}^i_{yz}(\vec{r}, \vec{r}') + \hat{z}\hat{y}\vec{G}^i_{zy}(\vec{r}, \vec{r}') + \hat{z}\hat{z}\vec{G}^i_{zz}(\vec{r}, \vec{r}')\end{aligned} \tag{2}$$

where the term $\vec{G}^i_{xy}(\vec{r}, \vec{r}')$ is the component of the electric Green's function associated with the $\hat{x}$ component of the electric field in region i due to the $\hat{y}$-directed component of the infinitesimal electric surface-current source $\vec{J}_s(r')$ located at $(x' = x_{01}, y', z')$. Other terms are defined similarly. The point current source $\vec{J}_s(r')$ is defined as

$$\vec{J}_s(r') = \hat{y}J_y + \hat{z}J_z = \Big[\delta(x - x_{01})\delta(y - y')\delta(z - z')\Big](\hat{y} + \hat{z}). \tag{3}$$

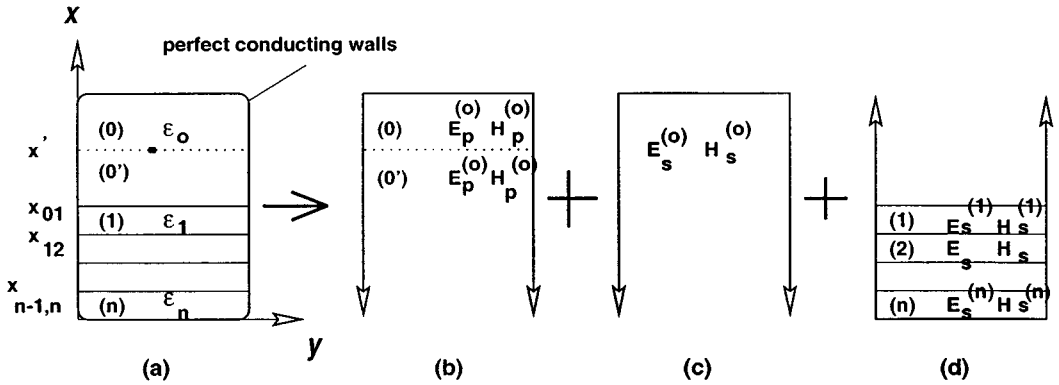

Fig. 2. Equivalent waveguide system that models an inhomogeneously loaded rectangular waveguide. The analysis uses a superposition of an equivalent set of parallel-plate structures.

The analysis is carried out by employing the principle of scattering superposition, which can be stated as follows. Assume that the EM fields or potentials for a given boundary value problem is known. If the boundary conditions change, the EM fields that satisfy the boundary conditions for the new structure are obtained by a superposition of the original known fields and a scattered one, which has the same spatial dependence as the original fields, but with unknown amplitudes. Imposing the new boundary conditions yield these unknown amplitudes. In Fig. 2, it is assumed that we have a certain boundary value problem depicted in Fig. 2(b). The solution to this problem is given by the primary fields E_p and H_p. The boundary conditions are then changed by adding a set of N layers of dielectrics and a bottom conducting wall [see Fig. 2(d)]. As a result, the fields in the overall guide change. This change is represented by a set of added fields E_s and H_s.

The procedure for deriving the Green's function for the cavity problem is mostly identical to that of the two-dimensional rectangular waveguide problem reported in [26], which was conducted to compute the propagation and dispersion characteristics of a uniform transmission line situated on top of lossy substrate comprised of N layers enclosed in a shielding rectangular waveguide. For the sake of brevity, this analysis will not be reproduced here. Using a similar approach, the Green's function for the cavity structure of Fig. 1 can be derived. For computing the fields around the discontinuity, only the Green's function in the region (0) above the metallization or the Green's function in the region (1) just below the metallization is required. The Green's function will be used to derive the electric fields tangential to the plane of the discontinuity. Hence, the evaluation of ${G_{xy}}^{(0)}$ and ${G_{xz}}^{(0)}$ is unnecessary. The mathematical task reduced to obtaining the remaining four components of the Green's function dyad: ${G_{yy}}^{(0)}$, ${G_{yz}}^{(0)}$, ${G_{zy}}^{(0)}$, and ${G_{zz}}^{(0)}$. These are found to be

$$G_{yy}^{(0)} = \sum_m \sum_n g_{yy_{mn}}^{(0)}(x) \cos\left(\frac{m\pi y}{b}\right) \cdot \cos\left(\frac{m\pi y'}{b}\right) \sin\left(\frac{n\pi z}{c}\right) \sin\left(\frac{n\pi z'}{c}\right) \quad (4)$$

$$G_{yz}^{(0)} = \sum_m \sum_n g_{yz_{mn}}^{(0)}(x) \cos\left(\frac{m\pi y}{b}\right) \cdot \sin\left(\frac{m\pi y'}{b}\right) \sin\left(\frac{n\pi z}{c}\right) \cos\left(\frac{n\pi z'}{c}\right) \quad (5)$$

$$G_{zy}^{(0)} = \sum_m \sum_n g_{zy_{mn}}^{(0)}(x) \sin\left(\frac{m\pi y}{b}\right) \cdot \cos\left(\frac{m\pi y'}{b}\right) \cos\left(\frac{n\pi z}{c}\right) \sin\left(\frac{n\pi z'}{c}\right) \quad (6)$$

$$G_{zz}^{(0)} = \sum_m \sum_n g_{zz_{mn}}^{(0)}(x) \sin\left(\frac{m\pi y}{b}\right) \cdot \sin\left(\frac{m\pi y'}{b}\right) \cos\left(\frac{n\pi z}{c}\right) \cos\left(\frac{n\pi z'}{c}\right) \quad (7)$$

where

$$g_{yy_{mn}}^{(0)}(x) = \varepsilon_{om}\left[\left(\frac{m\pi}{b}\right)^2 T_1 - \left(\frac{n\pi}{c}\right)^2 T_E(x_{01})\right] C(x) \quad (8)$$

$$g_{yz_{mn}}^{(0)}(x) = 2\left(\frac{m\pi}{b}\right)\left(\frac{n\pi}{c}\right)[T_1 + T_E(x_{01})]C(x) \quad (9)$$

$$g_{zy_{mn}}^{(0)}(x) = g_{yz_{mn}}^{(0)}(x) \quad (10)$$

and

$$g_{zz_{mn}}^{(0)}(x) = \varepsilon_{on}\left[\left(\frac{n\pi}{c}\right)^2 T_1 - \left(\frac{m\pi}{b}\right)^2 T_E(x_{01})\right] C(x) \quad (11)$$

where $\varepsilon_{o\nu}$ is defined as

$$\varepsilon_{o\nu} = \begin{cases} 1, & \text{if } \nu = 0 \\ 2, & \text{if } \nu \geq 1 \end{cases} \quad (12)$$

T_1, $C(x)$, T_M, and T_E are given by

$$T_1 = \frac{1}{{k_o}^2}\left[k_x^{(0)} k_x^{(1)} T_M(x_{01})\right] \quad (13)$$

$$C(x) = \frac{1}{b\left[\left(\frac{m\pi}{2}\right)^2 + k_z^2\right]} \frac{\sin k_x^{(0)}(a-x)}{\cos k_x^{(0)}(a-x_{01})} \quad (14)$$

$$T_M(x_{01}) = \frac{-1}{k_x^{(1)}\left(1 - \frac{a_{22}}{a_{12}} k_x^{(0)} \tan k_x^{(0)} d_0\right)} \quad (15)$$

and

$$T_E(x_{01}) = \frac{1}{k_x^{(0)} + \frac{b_{22}}{b_{12}} \tan k_x^{(0)} d_0} \quad (16)$$

where

$$a_{12} = k_x^{(1)}\left(K_{1_c} \sin k_x^{(1)} d_1 - K_{1_s} \cos k_x^{(1)} d_1\right) \quad (17)$$

$$a_{22} = \epsilon_{r_1}\left(K_{1_c} \cos k_x^{(1)} d_1 + K_{1_s} \sin k_x^{(1)} d_1\right) \quad (18)$$

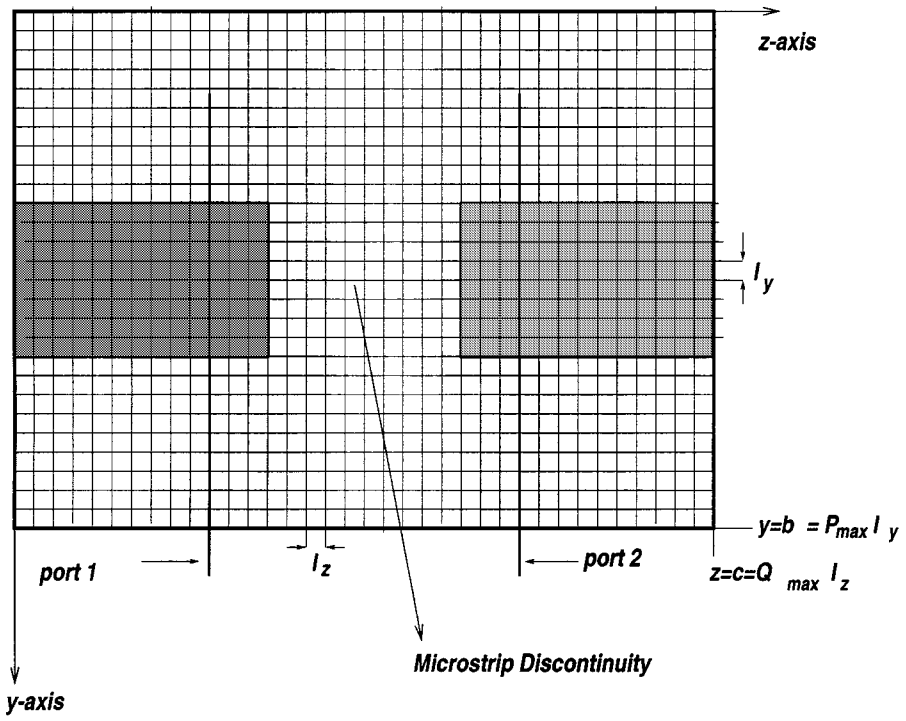

Fig. 3. Discretization of the discontinuity plane ($x = x_{01}$ plane).

$$b_{12} = \left(R_{1_s} \sin k_x^{(1)} d_1 + R_{1_c} \cos k_x^{(1)} d_1\right) \tag{19}$$

$$b_{22} = k_x^{(0)} \left(R_{1_s} \cos k_x^{(1)} d_1 - R_{1_c} \sin k_x^{(1)} d_1\right). \tag{20}$$

The terms R_{1_s}, R_{1_c}, K_{1_s}, and K_{1_c} are related recursively to R_{N-1_s}, R_{N-1_c}, K_{N-1_s}, and K_{N-1_c} through

$$K_{i-1_s} = \frac{k_x^{(i)}}{k_x^{(i-1)}} \left[K_{i_s} \cos\left(k_x^{(i)} d_i\right) - K_{i_c} \sin\left(k_x{}^{(i)} d_i\right)\right] \tag{21}$$

$$K_{i-1_c} = \frac{\epsilon_i}{\epsilon_{i-1}} \left[K_{i_s} \sin\left(k_x^{(i)} d_i\right) + K_{i_c} \cos\left(k_x^{(i)} d_i\right)\right] \tag{22}$$

$$R_{i-1_c} = \left[R_{i_s} \sin\left(k_x^{(i)} d_i\right) + R_{i_c} \cos\left(k_x^{(i)} d_i\right)\right] \tag{23}$$

and

$$R_{i-1_s} = \frac{k_x^{(i)}}{k_x^{(i-1)}} \left[R_{i_s} \cos\left(k_x^{(i)} d_i\right) - R_{i_c} \sin\left(k_x^{(i)} d_i\right)\right] \tag{24}$$

where

$$K_{N-1_c} = \frac{\epsilon_N}{\epsilon_{N-1}} \cos\left(k_x^{(N)} x_{N-1,N}\right) \tag{25}$$

$$K_{N-1_s} = \frac{k_x^{(N)}}{k_x^{(N-1)}} \sin\left(k_x^{(N)} x_{N-1,N}\right) \tag{26}$$

$$R_{N-1_s} = \frac{k_x^{(N)}}{k_x^{(N-1)}} \cos\left(k_x^{(N)} x_{N-1,N}\right) \tag{27}$$

and

$$R_{N-1_c} = \sin\left(k_x^{(N)} x_{N-1,N}\right). \tag{28}$$

III. Modeling of Microstrip Discontinuities

Consider now a certain metallization layout of arbitrary shape, perfect conductivity, and negligible thickness situated on top of the N layers of dielectrics. Consider a discontinuity in the metallization such as the series gap discontinuity depicted in Fig. 1. Again, as a result of adding this conducting geometry, the boundary conditions of the original cavity problem will change. Using the cavity Green's functions obtained earlier and using the current distribution on the metallization, the electric field is recalculated from the definition of electric Green's function subject to a new boundary condition; the tangential component of the electric field must vanish on the metallic strip.

The surface-current distribution for the discontinuity is unknown and is expressed in terms of a series of known basis functions with unknown amplitude coefficients. The electric field in the plane of the metallization is expressed in terms of these basis functions. Enforcing the boundary condition that $\vec{E} = 0$ on the metallization yields a system of linear equations whose unknowns are those unknown amplitude coefficients.

The surface-current density distribution is cast in the form

$$J_y(y', z') = \sum_{p'} \sum_{q'} I_{y_{p'q'}} f_{p'}(y') g_{q'}(z') \tag{29}$$

and

$$J_z(y', z') = \sum_{p'} \sum_{q'} I_{z_{p'q'}} g_{p'}(y') f_{q'}(z') \tag{30}$$

where $f_{p'}(y')g_{q'}(z')$ and $f_{q'}(z')g_{p'}(y')$ are basis function expansions for $J_y(y', z')$ and $J_z(y', z')$, respectively, with $I_{y_{p'q'}}$ and $I_{z_{p'q'}}$ being the unknown amplitude coefficients of $J_y(y', z')$ and $J_z(y', z')$, respectively. p' and q' are the summation integral indexes. The cavity dimensions b and c are

partitioned into $P_{\max}$ and $Q_{\max}$ segments, each of length l_y or l_z, respectively (see Fig. 3). The basis functions define the shape of the current within each subsection. Functions $f_{q'}(z')$ and $g_{p'}(y')$ are defined as

$$f_{q'}(z') = \begin{cases} \dfrac{\sin h_z(z_{q'+1} - z')}{\sin h_z l_z}, & \text{if } z_{q'} \le z' \le z_{q'+1} \\ \dfrac{\sin h_z(z' - z_{q'-1})}{\sin h_z l_z}, & \text{if } z_{q'} \le z' \le z_{q'} \\ 0, \quad \text{elsewhere} \end{cases} \tag{31}$$

and

$$g_{p'}(y') = \begin{cases} 1, & \text{if } y_{p'} - \dfrac{l_y}{2} \le y' \le y_{p'} + \dfrac{l_y}{2} \\ 0, & \text{elsewhere.} \end{cases} \tag{32}$$

h_z and h_y are the basis function wavenumbers. The above expansions and shaping functions have been previously applied to the problem of modeling microstrip discontinuities with excellent results obtained [24], [27]. The shape functions account for the edge effect on the current distribution. The coordinates $y_{p'}$ and $z_{q'}$ assume the following discrete coordinate values [28]:

$$y_{p'} = \begin{cases} p' l_y, & \text{in } J_y(y', z') \\ \left(p' + \dfrac{1}{2}\right) l_y, & \text{in } J_z(y', z') \end{cases} \tag{33}$$

$$z_{q'} = \begin{cases} \left(q' + \dfrac{1}{2}\right) l_z, & \text{in } J_y(y', z') \\ q' l_y, & \text{in } J_z(y', z'). \end{cases} \tag{34}$$

Since only the tangential component of the electric field is of interest at this point, only this component of the field will be evaluated. Those are the E_y and E_z components, which can be expressed in the form of two coupled integral equations

$$E_y^{(0)} = E_{yy}^{(0)} + E_{yz}^{(0)} \tag{35}$$

$$E_z^{(0)} = E_{yz}^{(0)} + E_{zz}^{(0)} \tag{36}$$

where, e.g., $E_{yy}^{(0)}$ is given by

$$E_{yy}^{(0)} = -j\omega\mu_o \iint G_{yy}^{(0)} J_y(y', z')\, dy'\, dz'. \tag{37}$$

The superscript (0) denotes the air-filled region of width d_0 above the cavity, as shown in Fig. 1. Expressions for $G_{yy}^{(0)}$, $G_{yz}^{(0)}$, $G_{zy}^{(0)}$, and $G_{zz}^{(0)}$ were derived in (4)–(7) and the expressions for $J_y(y', z')$ and $J_z(y', z')$ are given in (29) and (30) respectively. Hence, one arrives at [26]

$$\begin{aligned} E_{yy}^{(0)} = &- j\omega\mu_o l_y l_z \sum_{p'} \sum_{q'} I_{y_{p'q'}} \sum_m \sum_n g_{yy_{mn}}^{(0)} \\ &\cdot \left[\frac{\sin c\left[\dfrac{n\pi l_z}{2c}\right]}{\sin c(h_y l_y)} \right] \sin c\left[\left(\frac{m\pi}{b} + h_y\right)\frac{l_y}{2}\right] \\ &\cdot \sin c\left[\left(\frac{m\pi}{b} - h_y\right)\frac{l_y}{2}\right] \cos\left(\frac{m\pi y_{p'}}{b}\right) \\ &\cdot \sin\left(\frac{n\pi z_{q'}}{c}\right) \cos\left(\frac{m\pi y}{b}\right) \sin\left(\frac{n\pi z}{c}\right) \end{aligned} \tag{38}$$

$$\begin{aligned} E_{yz}^{(0)} = &- j\omega\mu_o l_y l_z \sum_{p'} \sum_{q'} I_{z_{p'q'}} \sum_m \sum_n g_{yz_{mn}}^{(0)} \\ &\cdot \left[\frac{\sin c\left[\dfrac{m\pi l_y}{2b}\right]}{\sin c(h_z l_z)} \right] \sin c\left[\left(\frac{n\pi}{c} + h_z\right)\frac{l_z}{2}\right] \\ &\cdot \sin c\left[\left(\frac{n\pi}{c} - h_z\right)\frac{l_z}{2}\right] \sin\left(\frac{m\pi y_{p'}}{b}\right) \\ &\cdot \cos\left(\frac{n\pi z_{q'}}{c}\right) \cos\left(\frac{m\pi y}{b}\right) \sin\left(\frac{n\pi z}{c}\right) \end{aligned} \tag{39}$$

$$\begin{aligned} E_{zy}^{(0)} = &- j\omega\mu_o l_y l_z \sum_{p'} \sum_{q'} I_{y_{p'q'}} \sum_m \sum_n g_{zy_{mn}}^{(0)} \\ &\cdot \left[\frac{\sin c\left[\dfrac{n\pi l_z}{2c}\right]}{\sin c(h_y l_y)} \right] \sin c\left[\left(\frac{m\pi}{b} + h_y\right)\frac{l_y}{2}\right] \\ &\cdot \sin c\left[\left(\frac{m\pi}{b} - h_y\right)\frac{l_y}{2}\right] \cos\left(\frac{m\pi y_{p'}}{b}\right) \\ &\cdot \sin\left(\frac{n\pi z_{q'}}{c}\right) \sin\left(\frac{m\pi y}{b}\right) \cos\left(\frac{n\pi z}{c}\right) \end{aligned} \tag{40}$$

$$\begin{aligned} E_{zz}^{(0)} = &- j\omega\mu_o l_y l_z \sum_{p'} \sum_{q'} I_{z_{p'q'}} \sum_m \sum_n g_{zz_{mn}}^{(0)} \\ &\cdot \left[\frac{\sin c\left[\dfrac{m\pi l_y}{2b}\right]}{\sin c(h_z l_z)} \right] \sin c\left[\left(\frac{n\pi}{c} + h_z\right)\frac{l_z}{2}\right] \\ &\cdot \sin c\left[\left(\frac{n\pi}{c} - h_z\right)\frac{l_z}{2}\right] \sin\left(\frac{m\pi y_{p'}}{b}\right) \\ &\cdot \cos\left(\frac{n\pi z_{q'}}{c}\right) \sin\left(\frac{m\pi y}{b}\right) \cos\left(\frac{n\pi z}{c}\right). \end{aligned} \tag{41}$$

IV. Method of Moments

The electric-field components $E_z^{(0)}$ and $E_y^{(0)}$ due to an arbitrary surface-current density distribution have been found. Enforcing the boundary condition $\vec{E_{\tan}} = 0$ on the perfectly conducting metallization yields the unknown amplitude coefficients. An equivalent boundary condition is that the conduction surface current and the tangential electric field are complementary quantities in the $x = x_{01}$ plane. Hence,

$$\iint E_y^{(0)} J_y\, dy\, dz|_{x=x_{01}} = \iint E_z^{(0)} J_z\, dy\, dz|_{x=x_{01}} = 0. \tag{42}$$

In a more explicit form

$$\begin{aligned} \iint_{\Delta s} E_y^{(0)} J_y\, dy\, dz &= \iint_{\Delta s} \left[E_{yy}^{(0)} + E_{yz}^{(0)}\right] J_y\, dy\, dz \\ &= \iint_{\Delta s} E_{yy}^{(0)} f_p(y) g_q(z)\, dy\, dz \\ &\quad + \iint_{\Delta s} E_{yz}^{(0)} f_p(y) g_q(z)\, dy\, dz \\ &= 0 \end{aligned} \tag{43}$$

and

$$\iint_{\Delta s} E_z^{(0)} J_z \, dy\, dz = \iint_{\Delta s} \left[E_{zy}^{(0)} + E_{zz}^{(0)}\right] J_z \, dy\, dz = \iint_{\Delta s} E_{zy}^{(0)} g_p(y) f_q(z)\, dy\, dz + \iint_{\Delta s} E_{yz}^{(0)} g_p(y) f_q(z)\, dy\, dz = 0 \tag{44}$$

where Δs is a segment on the plane $x = x_{01}$ with dimensions l_y and l_z in the y- and z-directions, respectively. Writing the above equations in the following short form:

$$\iint_{\Delta s} E_{yy}^{(0)} g_q(z) f_p(y)\, dy\, dz = \sum_{p'} \sum_{q'} I_{y_{p'q'}} Z_{yy}(p, q, p', q') \tag{45}$$

$$\iint_{\Delta s} E_{yz}^{(0)} g_q(z) f_p(y)\, dy\, dz = \sum_{p'} \sum_{q'} I_{z_{p'q'}} Z_{yz}(p, q, p', q') \tag{46}$$

$$\iint_{\Delta s} E_{zy}^{(0)} g_p(y) f_q(z)\, dy\, dz = \sum_{p'} \sum_{q'} I_{y_{p'q'}} Z_{zy}(p, q, p', q') \tag{47}$$

and

$$\iint_{\Delta s} E_{zz}^{(0)} g_p(y) f_q(z)\, dy\, dz = \sum_{p'} \sum_{q'} I_{z_{p'q'}} Z_{zz}(p, q, p', q') \tag{48}$$

the system of equations (43) and (44) can be written in the following matrix form:

$$\begin{pmatrix} Z_{yy}(p, q, p', q') & Z_{yz}(p, q, p', q') \\ Z_{zy}(p, q, p', q') & Z_{zz}(p, q, p', q') \end{pmatrix} \begin{pmatrix} I_y(p', q') \\ I_z(p', q') \end{pmatrix} = \begin{pmatrix} V_y(p, q) \\ V_z(p, q) \end{pmatrix}. \tag{49}$$

The elements of the left-hand-side (LHS) matrix of the above system need not be evaluated at all segments Δs of the plane $x = x_{01}$. The coefficients matrix can be evaluated only for the metallized segments of that plane since the conduction current is, by definition, zero everywhere else. Using (38)–(41) in (45)–(48), the coefficients $Z_{yy}(p, q, p', q')$, $Z_{yz}(p, q, p', q')$, $Z_{zy}(p, q, p', q')$ and $Z_{zz}(p, q, p', q')$ are obtained as [26]

$$Z_{yy}(p, q, p', q') = \sum_{m=1}^{m=M} \sum_{n=1}^{n=N} g_{yy_{mn}}^{(0)} \left[\frac{\sin c\left(\frac{n\pi l_z}{2c}\right)}{\sin c(h_y l_y)}\right]^2 \cdot \left[\sin c\left(\left(\frac{m\pi}{b} + h_y\right)\frac{l_y}{2}\right) \sin c\left(\left(\frac{m\pi}{b} - h_y\right)\frac{l_y}{2}\right)\right]^2 \cdot \cos\left(\frac{m\pi y_{p'}}{b}\right) \sin\left(\frac{n\pi z_{q'}}{c}\right) \cos\left(\frac{m\pi y}{b}\right) \sin\left(\frac{n\pi z}{c}\right) \tag{50}$$

$$Z_{yz}(p, q, p', q') = \sum_{m=1}^{m=M} \sum_{n=1}^{n=N} g_{yz_{mn}}^{(0)} \left[\frac{\sin c\left(\frac{n\pi l_z}{2c}\right)}{\sin c(h_y l_y)}\right] \left[\frac{\sin c\left(\frac{m\pi l_y}{2b}\right)}{\sin c(h_z l_z)}\right] \cdot \left[\sin c\left(\left(\frac{m\pi}{b} + h_y\right)\frac{l_y}{2}\right) \sin c\left(\left(\frac{m\pi}{b} - h_y\right)\frac{l_y}{2}\right)\right] \cdot \left[\sin c\left(\left(\frac{n\pi}{c} + h_z\right)\frac{l_z}{2}\right) \sin c\left(\left(\frac{n\pi}{c} - h_z\right)\frac{l_z}{2}\right)\right] \cdot \sin\left(\frac{m\pi y_{p'}}{b}\right) \cos\left(\frac{n\pi z_{q'}}{c}\right) \cos\left(\frac{m\pi y}{b}\right) \cos\left(\frac{n\pi z}{c}\right) \tag{51}$$

$$Z_{zy}(p, q, p', q') = Z_{yz}(p', q', p, q) \tag{52}$$

and

$$Z_{zz}(p, q, p', q') = \sum_{m=1}^{m=M} \sum_{n=1}^{n=N} g_{zz_{mn}}^{(0)} \left[\frac{\sin c\left(\frac{m\pi l_y}{2b}\right)}{\sin c(h_z l_z)}\right]^2 \cdot \left[\sin c\left(\left(\frac{n\pi}{c} + h_z\right)\frac{l_z}{2}\right) \sin c\left(\left(\frac{n\pi}{b} - h_z\right)\frac{l_z}{2}\right)\right]^2 \cdot \cos\left(\frac{m\pi y_{p'}}{b}\right) \sin\left(\frac{n\pi z_{q'}}{c}\right) \sin\left(\frac{m\pi y}{b}\right) \cos\left(\frac{n\pi z}{c}\right). \tag{53}$$

The summation over m and n is truncated at $m = M < \infty$ and $n = N < \infty$, respectively. The truncation at M and N is chosen such that the retained terms provide sufficiently accurate results. Criteria for choosing M and N are presented later.

The matrix of (49) is a system of linear equations obtained from the boundary condition of equation (42). It follows that the right-hand side (RHS) of the system (49) is a vector of zeros. However, that boundary condition is violated at one or more points to provide an excitation to the system. Hence, $V_y(p, q)$ and $V_z(p, q)$ are termed the excitation vectors. For a given excitation vector, a certain current distribution is maintained on the metallization. That distribution is given by the amplitude coefficients $I_y(p', q')$ and $I_y(p', q')$. The point at which $V_y(p, q) \neq 0$ or $V_y(p, q) \neq 0$ is called the gap generator. Hence, $V_y(p, q)$ and $V_y(p, q)$ are defined as [29]

$$V_y(p, q) = \begin{cases} 1, & \text{if } y_p = y_{\text{gap}} \\ 0, & \text{elsewhere on the metallization} \end{cases} \tag{54}$$

$$V_z(p, q) = \begin{cases} 1, & \text{if } z_q = z_{\text{gap}} \\ 0, & \text{elsewhere on the metallization.} \end{cases} \tag{55}$$

The gap generator excitation method [30], [29] is a nonphysical mathematical tool to excite the circuit. Another technique to excite the circuit is the cavity resonance technique [31], [32], which, again, is a pure mathematical tool. A coaxial excitation method is developed in [22], which has its physical foundation in modeling the feed current of a coaxial line leading to the microstrip. The end result, however, is independent of the excitation method.

V. Numerical Implementation

A. Matrix Computation and Inversion

It is important to note the following symmetries in the impedance matrix:

$$Z_{yy}(p, q, p', q') = Z_{yy}(p', q', p, q) \tag{56}$$

$$Z_{zz}(p, q, p', q') = Z_{zz}(p', q', p, q) \tag{57}$$

and

$$Z_{zy}(p, q, p', q') = Z_{yz}(p', q', p, q). \tag{58}$$

These symmetries are utilized to reduce the computational effort in the calculation of matrix elements by about 50% [To be exact, the ratio of the number of elements that needs to be evaluated to the total number of elements in the matrix is reduced to $0.5*(1+1/N)$]. Based on computational experiences, computing the matrix elements consumes over 99% of the computation time, with the remaining 1% used for the matrix solution. These symmetries also reduce the size of the storage array in half.

For the case of a narrow strip of metallization along the z-axis, and where the discontinuity does not lead to a large y-directed current, a subset of this matrix can be used. For example, when characterizing a series gap discontinuity in a thin transmission line, the I_y component of current was found to be of negligible magnitude compared to the I_z component. Hence, it is sufficient to only consider the problem

$$\Big(Z_{zz}(p, q, p', q')\Big)\Big(I_z(p', q')\Big) = \Big(V_z(p, q)\Big). \tag{59}$$

B. Parameters Extraction

It is assumed that a uniform transmission line feeds a discontinuity from all ports. For a two-port problem, the longitudinal currents I_{z_1} and I_{z_2} on ports 1 and 2 are evaluated using $I_z(p', q')$ by a transverse integration. At the input port, on a uniform transmission line, an ideal transmission-line current exists as long as the operating frequency is below the cutoff frequency of the shielding cavity. Thus, the current distribution obtained can be fit to a transmission-line current model to obtain the scattering parameters. The current distribution obtained behaves like a transmission-line model away from the excitation point and the discontinuity itself (say, by a distance of $d_s = (\lambda_g/4)$ from each).

An ideal transmission line current is given by

$$I_z = I_z^+ e^{-j\beta_z z} + I_z^- e^{j\beta_z z} \tag{60}$$

where I_z^+ is the incident current, I_z^- is the reflected current, and β_z is the complex propagation constant. The optimization routine used for the fitting purpose is L-BFGS-B [33]. The error function supplied to the routine for minimization is

$$E = \left[\mathrm{Re}\left(I_{z_{\mathrm{computed}}} - I_{z_{\mathrm{ideal}}}\right)\right]^2 + \left[\mathrm{Im}\left(I_{z_{\mathrm{computed}}} - I_{z_{\mathrm{ideal}}}\right)\right]^2. \tag{61}$$

Minimizing this error function yields the unknown parameters in (60), namely, I_z^+, I_z^- and β_z. A strength of this theory is that it does not require the knowledge of β_z on the feed transmission lines to solve the discontinuity problem. From the information obtained by the optimization routine, the voltage reflection coefficient for the input port Γ_{in} is

$$\Gamma_{\mathrm{in}} = \frac{I_z^-}{I_z^+} e^{j2\beta_z(L+d_s-d_{\mathrm{ref}})} \tag{62}$$

where d_{ref} is the reference plane distance.

C. Scattering and Impedance Matrices

For a one-port discontinuity, the scattering parameter S_{11} is given by the reflection coefficient in (62). For a symmetric two-port geometry, two excitations are required: an even and odd excitation. For an even excitation, the gap generators of (55) are equal to one on both ends, and zero everywhere else on the metallization. For an odd excitation, the gap generator of (55) is equal to one at one end and to -1 at the other end. Using these two excitations, two different reflection coefficients are computed: $\Gamma_{\mathrm{in}}^{\mathrm{even}}$ and $\Gamma_{\mathrm{in}}^{\mathrm{odd}}$. The normalized input impedance for the even and odd excitations are given by

$$Z_{\mathrm{in}}^{\mathrm{even}} = \frac{1+\Gamma_{\mathrm{in}}^{\mathrm{even}}}{1-\Gamma_{\mathrm{in}}^{\mathrm{even}}} \tag{63}$$

$$Z_{\mathrm{in}}^{\mathrm{odd}} = \frac{1+\Gamma_{\mathrm{in}}^{\mathrm{odd}}}{1-\Gamma_{\mathrm{in}}^{\mathrm{odd}}}. \tag{64}$$

From microwave-circuit theory, and considering a two-port network symmetric impedance matrix representation, the following relationships are obtained:

$$Z_{11} = \frac{Z_{\mathrm{in}}^{\mathrm{even}} + Z_{\mathrm{in}}^{\mathrm{odd}}}{2} \tag{65}$$

$$Z_{12} = \frac{Z_{\mathrm{in}}^{\mathrm{even}} - Z_{\mathrm{in}}^{\mathrm{odd}}}{2}. \tag{66}$$

The scattering matrix $[S]$ is related to the impedance matrix $[Z]$ through

$$S_{11} = S_{22} = \frac{Z_{11}^2 - Z_{12}^2 - 1}{Z_{11}^2 - Z_{12}^2 + 2Z_{11} + 1} \tag{67}$$

$$S_{12} = S_{21} = \frac{2Z_{12}}{Z_{11}^2 - Z_{12}^2 + 2Z_{11} + 1}. \tag{68}$$

D. Convergence Consideration

Detailed convergence and verification studies were conducted in [24] for the same theory, but for the special case of a two-layered substrate. These were also conducted in [21] for a closely related analysis. These criteria were tested and verified in the current analysis for the case of N-layered substrate. For discontinuity analysis, the convergence criteria depend on the modal summation limits M and N, the subsection highest indexes P and Q, the cavity dimensions a, b, and c, the subsection lengths l_z and l_y, and the subsection wavenumbers h_y and h_z. These convergence criteria can be summarized as follows.

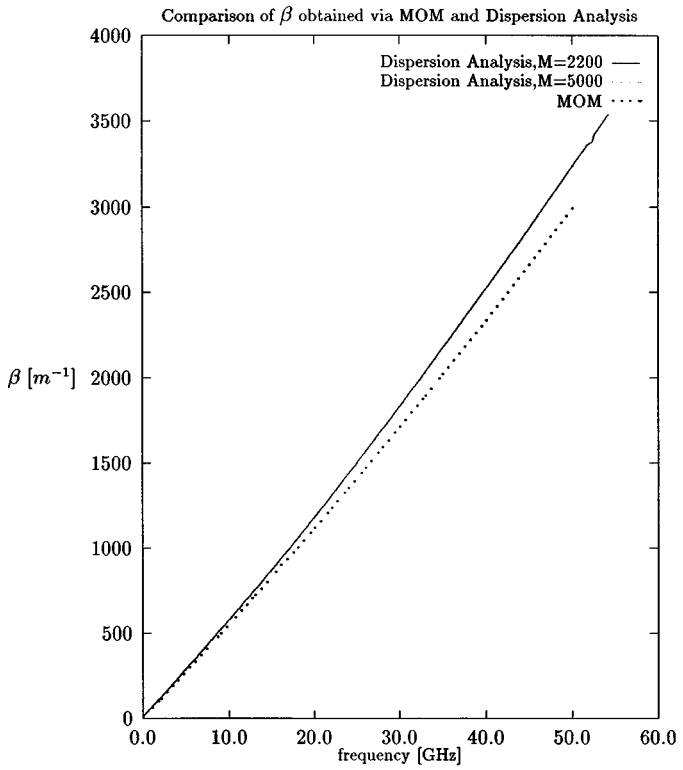

Fig. 4. Propagation constant β (m^{-1}) versus frequency f (GHz) for a uniform transmission line. Comparison of the results obtained via the MoM presented in this paper and that obtained via direct dispersion analysis [26]. MoM computation conducted using $M \times N = 300 \times 300$ modes. Direct dispersion analysis [26] is conducted for two cases: $M = 2200$ modes and 5000 modes. Transmission-line parameters are: width $W = 0.5$ mm, shield dimensions: $a = 6$ mm, and $b = 1.5$ mm. The substrate is comprised of two layers, one with a thickness 0.2 mm, $\epsilon_r = 12$ and $\rho = 1.2\ \Omega \cdot$ m and below it an insulating layer of thickness 0.2 mm and $\epsilon_r = 12$.

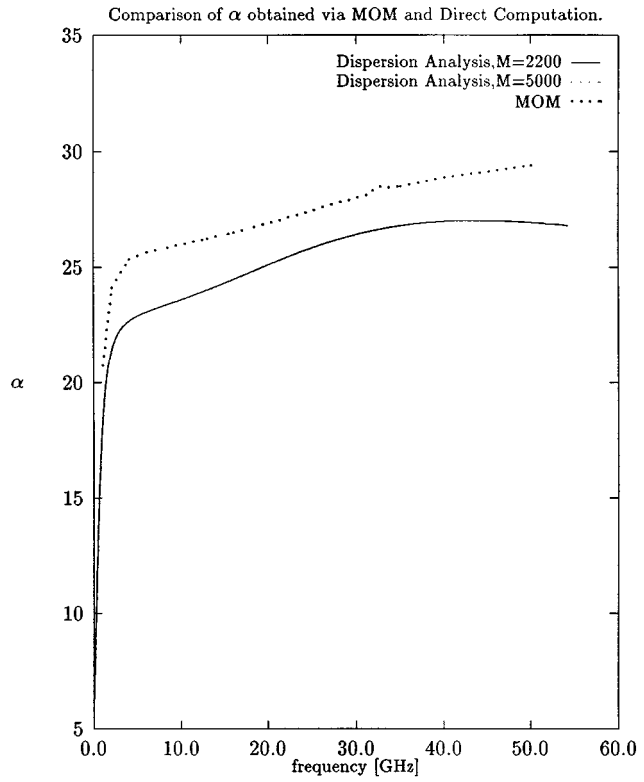

Fig. 5. Attenuation constant α (m^{-1}) versus frequency f (GHz). The analysis presented in this paper (i.e., MoM) is compared to that of [26]. All parameters are as per Fig. 4.

1) The dimensions of the enclosing cavity must be such that its lowest cutoff frequency is higher than the highest frequency with which the discontinuity is excited. Otherwise, if the cavity were to resonate at a certain frequency, coupling could occur between the microstrip circuit and resonant cavity.
2) Based on extensive numerical testing carried out in [21], choosing the subsection wavenumbers h_y and h_z to be approximately equal to the phase constant of the microstrip feed lines yield the best results.
3) To guarantee convergent accurate results, and due to the nature of the overlapping sinusoidal basis functions, the maximum value for l_z and l_y is governed by $h_z l_z,\ h_y l_y \leq (\pi/2)$.
4) Based on computing experience, the relationship between the modal summation limits M and N and the subsection highest indexes P and Q should be $M \geq 1.25P$ and $N \geq 1.25Q$. The same criterion was observed in [22] and [34].
5) For accurate results, the values of l_y and l_z should be such that $(\lambda_g/175) \leq l_y,\ l_z \leq (\lambda_g/25)$, where λ_g is the guided wavelength. If l_y and l_z are greater than $(\lambda_g/25)$, inaccurate results for the current distribution are obtained due to insufficient sampling points per wavelength. If $l_y,\ l_z$ are smaller than $(\lambda_g/175)$, inaccurate results for the current distribution are again obtained. This time, the source of error is that the adjacent matrix elements of (49) have very close values, leading to a reduced numerical accuracy during the matrix solution. This condition is not absolute, but recommended.

VI. Model Verification and Examples

In this section, the current method of moments (MoM) analysis is verified using a uniform transmission-line problem. This analysis is compared to the dispersion analysis for a uniform transmission line reported in [26]. A discontinuity in the same transmission line is then considered. As an example of a discontinuity, a series gap is studied as per Fig. 1. The discontinuity results are compared to a quasi-TEM analysis [6].

Fig. 4 depicts the frequency dependence of the propagation constant β for a uniform transmission line of width $W = 0.5$ mm and a silicon substrate of thickness 0.4 mm. The substrate is comprised of two layers, one with a relative permittivity $\epsilon_r = 12$, resistivity $\rho = 1.2\ \Omega$m, and a thickness of 0.2 mm, and beneath it there is an insulating layer of relative permittivity $\epsilon_r = 12$. The shielding rectangular waveguide dimensions are $a = 6$ mm and $b = 1.5$ mm. First, computation were conducted using the dispersion analysis for a uniform transmission line reported in [26]. Two values for the summation index M were considered: $M = 2200$ modes and $M = 5000$ modes. The two results fully overlap. The

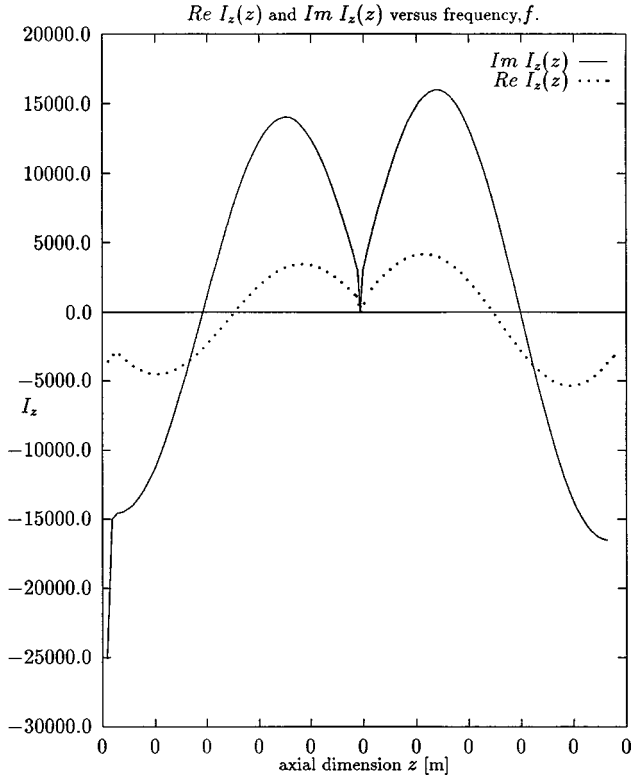

Fig. 6. Axial current $I_z(z)$ versus z at $f = 9$ GHz for an even excitation. All parameters as per Fig. 4.

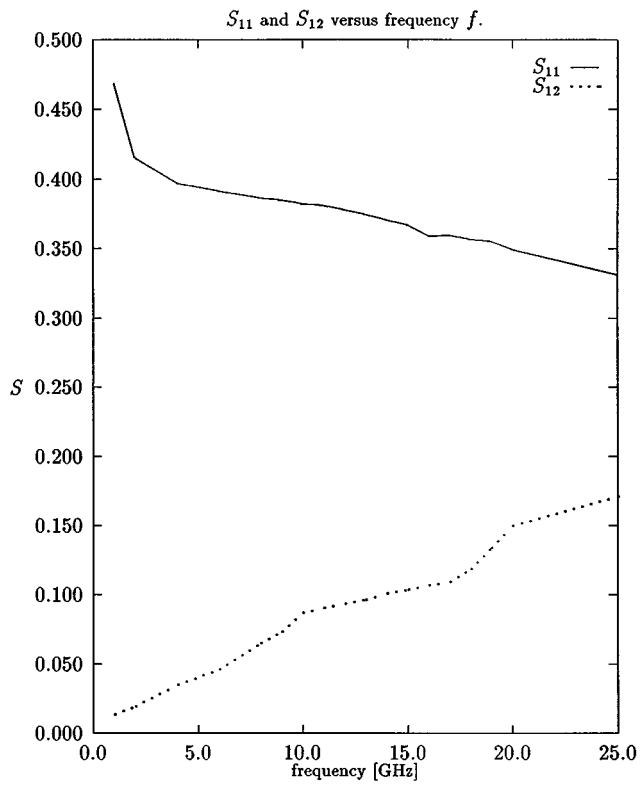

Fig. 7. Scattering matrix elements S_{11} and S_{12} versus frequency f (GHz). All parameters are as per Fig. 4.

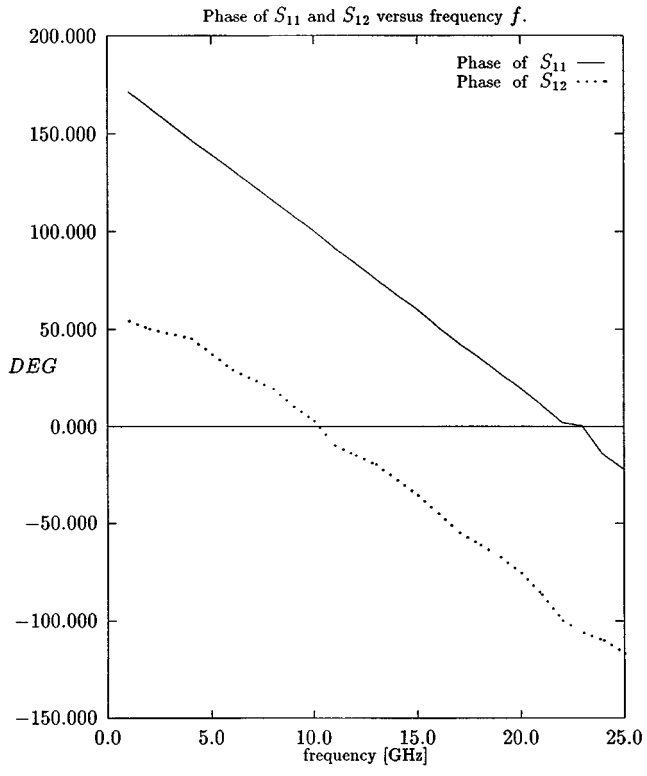

Fig. 8. The phase of S_{11} and S_{12} of the gap versus frequency f (GHz). All parameters are as per Fig. 4.

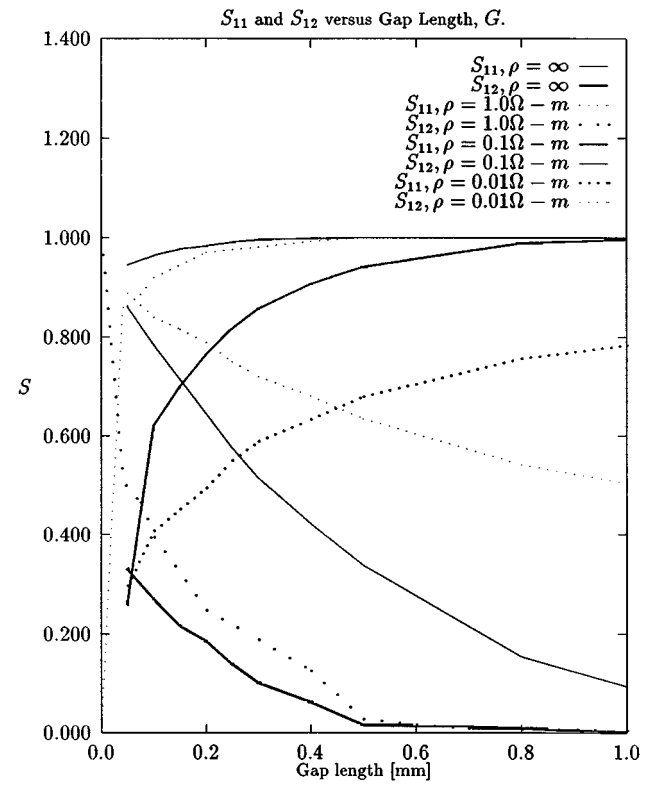

Fig. 9. Scattering matrix elements S_{11} and S_{12} versus gap length G (mm) at $f = 20$ GHz. All parameters are as per Fig. 4.

attenuation constant α versus frequency f for this transmission line is shown in Fig. 5.

Second, the analysis presented here was utilized to study the same uniform transmission line. The numerical computation is

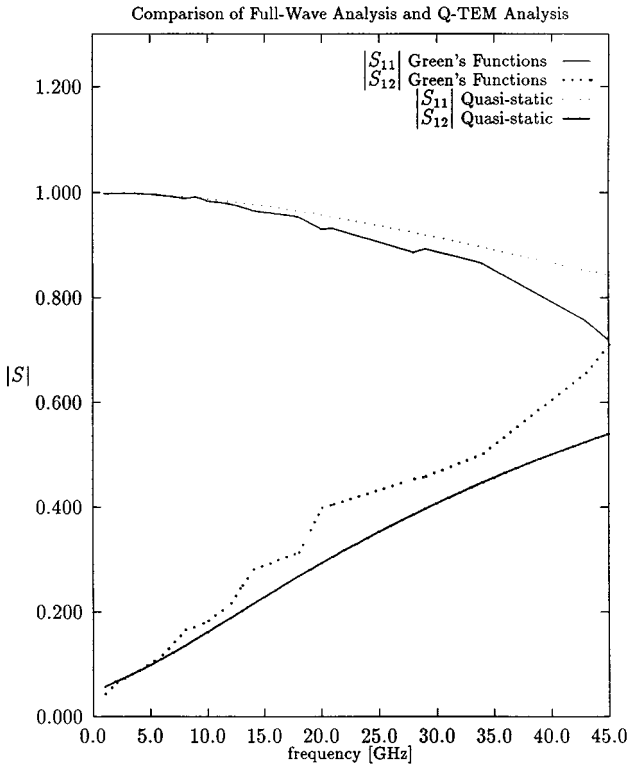

Fig. 10. Deembedded scattering matrix elements S_{11} and S_{12} of the gap versus frequency f (GHz). All parameters are as per Fig. 4.

conducted using $M = 300$ and $N = 300$ for a cavity of length $c = 20$ mm, with subsection discretization of $P = 300$ and $Q = 300$. Results are also shown in Figs. 4 and 5. Minor deviations between the two theories are attributed to the difference between the two-dimensional uniform transmission-line model of [26], as compared to the three-dimensional short transmission line enclosed in the cavity, as modeled by the current MoM theory.

A typical axial current distribution $I_z(z)$ along the propagation direction z at $f = 9$ GHz for the given transmission line with a series gap of length 0.1 mm is shown in Fig. 6 for the case of even excitation. The real component of the current is the one associated with the loss in the transmission line. For a lossless transmission line, the axial current is 90° out of phase with the excitation.

The magnitude of the scattering matrix elements S_{11} and S_{12} versus frequency is shown in Fig. 7 for the case of a series gap of length 0.1 mm in the middle of the transmission. The phase of S_{11} and S_{12} versus frequency is depicted in Fig. 8. The magnitude of S_{11} and S_{12} versus the gap length for a fixed frequency of 20 GHz for a variety of substrate conductivities is shown in Fig. 9.

The scattering matrix elements for the gap are deembedded from the data of Figs. 7 and 8 by placing the reference planes on both sides of the discontinuity at a distance 1.05 mm from the center of the discontinuity. These results are depicted in Fig. 10. Comparisons with results obtained using a quasi-TEM theory for modeling the gap [6] are also depicted in Fig. 10. Quasi-TEM analysis shows a good agreement with the current full-wave analysis up to about 10 GHz. At higher frequencies, quasi-TEM analysis becomes less accurate, as it underestimates the coupling through the gap.

VII. Conclusion

In this paper, a rigorous theory for analyzing discontinuities in a shielded transmission-line structures has been developed. This analysis can model multilayered lossy substrates and multiconductor structures. The analysis is based on a Green's function formulation in the space domain. This was achieved through an extension of an analytical approach reported earlier in the literature for a two-layered substrate [24]. A notable strength of this approach is that the mathematical complexity of the problem does not greatly increase with the number of substrate layers. The validity and accuracy of this method were established through comparison with other modeling approaches. Convergence criteria are outlined and verified.

References

[1] J. R. Wait, *Electromagnetic Waves in Stratified Media*. Oxford, U.K.: Institute of Electrical and Electronics Engineers, Oxford Univ. Press, 1996.
[2] A. Bhattacharyya, *Electromagnetic Fields in Multilayered Structures: Theory and Applications*. Norwood, MA: Artech House, 1994.
[3] J. B. Faria, *Multiconductor Transmission-Line Structures, Modal Analysis Techniques*, ser. Microwave Opt. Eng. New York: Wiley, 1993.
[4] H. A. Wheeler, "Transmission line properties of parallel wide strips by conformal mapping approximation," *IEEE Trans. Microwave Theory Tech.*, vol. MTT-12, pp. 280–289, Feb. 1964.
[5] ——, "Transmission line parallel strips separated by a dielectric sheet," *IEEE Trans. Microwave Theory Tech.*, vol. MTT-13, pp. 172–185, Jan. 1965.
[6] M. Maeda, "An analysis of gap in microstrip transmission lines," *IEEE Trans. Microwave Theory Tech.*, vol. MTT-20, pp. 390–396, Feb. 1972.
[7] P. Benedek and P. Silvester, "Equivalent capacitances for microstrip gaps and steps," *IEEE Trans. Microwave Theory Tech.*, vol. MTT-20, pp. 729–733, Apr. 1972.
[8] R. Garg and I. J. Bahl, "Microstrip discontinuities," *Int. J. Electron.*, vol. 45, pp. 81–87, 1978.
[9] E. Yamashita and R. Mittra, "Variational method for the analysis of microstrip lines," *IEEE Trans. Microwave Theory Tech.*, vol. MTT-16, pp. 251–256, Feb. 1968.
[10] P. Silvester, "TEM properties of microstrip lines," *Proc. IEEE*, vol. 115, pp. 42–49, Jan. 1968.
[11] S. Nam, H. Ling, and T. Itoh, "Time domain method of lines applied to planar guide structures," *IEEE Trans. Microwave Theory Tech.*, vol. 37, pp. 897–901, May 1989.
[12] Z. Chen and B. Gao, "Full-wave analysis of multiconductor coupled lines in MIC's by the method of lines," *Proc. Inst. Elect. Eng.*, pt. H, vol. 136, no. 5, pp. 1171–1175, Oct. 1989.
[13] N. Georgieva and E. Yamashita, "Time domain vector-potential analysis of transmission-line problems," *IEEE Trans. Microwave Theory Tech.*, vol. 46, pp. 404–410, Apr. 1998.
[14] X. Zhang and K. Mei, "Time-domain finite difference approach to a calculation of the frequency-dependent characteristics of microstrip discontinuities," *IEEE Trans. Microwave Theory Tech.*, vol. 36, pp. 1775–1787, Dec. 1988.
[15] D. Bica and B. Beker, "Analysis of microstrip discontinuities using the spatial network method with absorbing boundary conditions," *IEEE Trans. Microwave Theory Tech.*, vol. 44, pp. 1157–1161, July 1996.
[16] W. J. R. Hoefer, "The transmission line matrix method-theory and applications," *IEEE Trans. Microwave Theory Tech.*, vol. MTT-33, pp. 882–893, May 1985.
[17] C. Tzuang and T. Itoh, "Finite element analysis of slow-wave Schottky contact printed lines," *IEEE Trans. Microwave Theory Tech.*, vol. MTT-34, pp. 1483–1489, Dec. 1986.
[18] G. Hughes and R. White, "MIS and Schottky barrier microstrip devices," *Proc. IEEE*, vol. 60, pp. 1460–1461, Dec. 1972.

[19] H. Hasegawa and S. Seki, "Analysis of interconnection delay on very high-speed LSI/VLSI chips using an MIS microstrip line model," *IEEE Trans. Microwave Theory Tech.*, vol. MTT-32, pp. 1721–1727, Oct. 1984.
[20] S. Sali, "Modeling of resistive and geometrical discontinuities in microstrip interconnections on integrated circuits," *Proc. Inst. Elect. Eng.*, pt. H, vol. 137, pp. 728–736, May 1990.
[21] L. P. Dunleavy and P. B. Katehi, "Shielding effects in microstrip discontinuities," *IEEE Trans. Microwave Theory Tech.*, vol. 36, pp. 1767–1774, Dec. 1988.
[22] ——, "A generalized method for analyzing shielded thin microstrip discontinuities," *IEEE Trans. Microwave Theory Tech.*, vol. 36, pp. 1758–1766, Dec. 1988.
[23] T. G. Livernois and P. B. Katehi, "A generalized method for deriving the space-domain Green's function in a shielded, multilayer substrate structure with applications to MIS slow-wave transmission lines," *IEEE Trans. Microwave Theory Tech.*, vol. 37, pp. 1761–1767, Nov. 1989.
[24] ——, "A simple method for characterizing planar transmission line discontinuities on dissipative substrates," *IEEE Trans. Microwave Theory Tech.*, vol. 39, pp. 368–370, Feb. 1991.
[25] T. E. Van Deventer, P. B. Katehi, and A. C. Cangellaris, "An integral equation method for evaluation of conductor and dielectric losses in high frequency interconnects," *IEEE Trans. Microwave Theory Tech.*, vol. 37, pp. 1964–1972, Dec. 1989.
[26] E. S. Tony, "Electromagnetic modeling of integrated optical wave controlled microstrip discontinuities," Ph.D. dissertation, Dept. Elect. Eng., Univ. Waterloo, Waterloo, ON, Canada, 1998.
[27] W. P. Harokopus and L. P. B. Katehi, "Electromagnetic coupling and radiation loss considerations in microstrip (M)MIC design," *IEEE Trans. Microwave Theory Tech.*, vol. 39, pp. 413–421, Mar. 1991.
[28] M. F. Catedra, J. G. Cuevas, and L. Nuno, "A scheme to analyze conducting plates of resonant size using the conjugate-gradient method and the fast Fourier transform," *IEEE Trans. Antennas Propagat.*, vol. 36, pp. 1744–1752, Dec. 1988.
[29] J. C. Rautio and R. F. Harrington, "An electromagnetic time–harmonic analysis of shielded microstrip circuits," *IEEE Trans. Microwave Theory Tech.*, vol. MTT-35, pp. 726–730, Aug. 1987.
[30] P. B. Katehi and N. Alexopoulos, "Microstrip discontinuity modeling for millimetric integrated circuits," in *IEEE MTT-S Microwave Symp. Dig.*, vol. 2, 1985, pp. 571–573.
[31] R. H. Jansen, "Hybrid mode analysis of end effects of planar microwave and millimeter-wave transmission lines," *Proc. IEEE*, vol. 128, pp. 77–86, Jan. 1981.
[32] T. Itoh, "Analysis of microstrip resonators," *IEEE Trans. Microwave Theory Tech.*, vol. MTT-24, pp. 946–951, June 1974.
[33] C. Zhu, R. H. Byrd, P. Lu, and J. Nocedal, "L-BFGS-B: FORTRAN subroutine for large-scale bound constrained optimization," Dept. EECS, Northwestern Univ., Evanston, IL, Tech. Rep. NAM12, Oct. 1996.
[34] W. Wertgen and R. H. Jansen, "Efficient direct and iterative electrodynamic analysis of geometrically complex MIC and MMIC structures," *Int. J. Numer. Modeling*, vol. 2, pp. 153–186, 1989.

Essam S. Tony (S'90–M'98) was born in Cairo, Egypt, on May 3, 1968. He received the B.Sc. degree (with honors) in electronics and communications from Ain Shams University, Cairo, Egypt, in 1991, and the M.A.Sc. and Ph.D. degrees in electrical engineering from the University of Waterloo, Waterloo, ON, Canada in 1993 and 1998, respectively. His M.A.Sc. research focused on the area of acoustooptical filters, and his doctoral research focused on the area of optical control of microstrip multilayered circuits.

Since May 1998, he has been with the Optical Systems Analysis Group, Nortel Networks, Saint John, NB, Canada, where he is responsible for defining and modeling the optical system performance for 10- and 40-Gb/s within the Research and Development Organization, Global High Capacity Optical Transport Division. His current research interest includes nonlinear propagation in optical fibers and optical systems modeling and analysis.

Sujeet K. Chaudhuri (M'79–SM'85) was born in Calcutta, India, on August 25, 1949. He received the B.E. degree (with honors) in electronics engineering from the Birla Institute of Technology and Science (BITS), Pilani, India, in 1970, the M.Tech. degree in electrical communication engineering from the Indian Institute of Technology (IIT), Delhi, India, in 1972, and the M.A.Sc. degree in microwave engineering and the Ph.D. degree in EM theory from the University of Manitoba, Winnipeg, MB, Canada, in 1973 and 1977, respectively.

In 1977 he joined the University of Waterloo, Waterloo, ON, Canada, where he is currently a Professor in the Electrical and Computer Engineering Department and the Dean of the Faculty of Engineering. He was a Visiting Associate Professor in the Electrical Engineering and Computer Science Department, University of Illinois at Chicago (1981 and 1984), a Visiting Professor at the National University of Singapore (1990–1991), and a Erskine Fellowship at the University of Canterbury, Canterbury, New Zealand (1998). He has been involved in contract research and consulting work with several Canadian and U.S. industries and government research organizations. His current research interests are in guided-wave/electrooptic structures, planar microwave structures, dielectric resonators, optical and EM imaging, and the fiber-based broad-band network.

Dr. Chaudhuri is a member of URSI Commission B and Sigma Xi.